Slip-flow and heat transfer in rectangular microchannels in the presence of thermal creep

H. Niazmand[1], M. Renksizbulut[2], A. Amiri Jaghargh[1]

[1] *Ferdowsi University of Mashhad, Mechanical Engineering Department, Mashhad, Iran*

[2] *University of Waterloo, Mechanical & Mechatronics Engineering Department, Waterloo, Ontario, Canada, N2L 3G1*

Email: *hniazmand@yahoo.com*

ABSTRACT

A control-volume numerical approach has been used to study rarefaction effects in simultaneously hydrodynamically and thermally developing 3D micro flows in rectangular channels for Kn ≤ 0.1. The effects of velocity slip, thermal creep and temperature jump on the key flow parameters are examined in detail. Low Reynolds number flows (Re ≤ 1) for different channel aspect ratios ($0 \le \alpha^* \le 1$) are considered. The effects of rarefaction on the global features of the flow and thermal development in the entrance region are studied. Dramatic reductions in the friction coefficient are observed in the entrance region due to rarefaction effects, which are enhanced by thermal creep. For the fluid heating case considered here, thermal creep increases slip at the wall and thereby further reduces the friction coefficient and enhances heat transfer. For an identical heat flux applied to the microchannel walls, thermal creep effects become more pronounced at lower Reynolds numbers since it results in higher axial temperature gradients. Present results for Kn = 0.1 indicate that the flow and thermal fields are greatly influenced by thermal creep at Re = 0.1.

1. INTRODUCTION

Increasing the power density and compactness of electronic devices requires efficient and powerful heat sinks in order to maintain their working temperature at acceptable levels. It has been shown that extremely high heat fluxes (as high as 790 W/cm^2) can be dissipated by microchannel heat sinks [1, 2]. Furthermore, the advantages of miniaturization in various micro-electro-mechanical systems for bioengineering, fuel cell technologies, lab-on-a-chip, etc., emphasize the role of microchannels as key components of associated devices. Normally, ducts with hydraulic diameters (D_h) less than 100 μm are considered microchannels.

An important effect associated with gas flows in microchannels is the rarefaction effect. Rarefaction can occur either at low-pressures where the molecular mean free path (λ) is large, or in micro devices at normal pressures if the characteristic length scale is small. In either case, the Knudsen number (Kn) which is defined as the ratio of λ to the appropriate length scale of the flow, becomes considerable. For Kn < 10^{-3}, the classical continuum approach is valid. For Knudsen numbers in the range 10^{-3} < Kn < 0.1 which is called the slip-flow regime, the standard Navier-Stokes and energy equations can accurately predict the flow features only when appropriate velocity-slip and temperature-jump boundary conditions are specified at the walls.

Slip-flow heat transfer in straight microchannels of arbitrary cross section has been the subject of numerous studies in the past. Hooman [3] developed an analytical approach to investigate fully developed (both hydrodynamically and thermally) flows in microchannels of arbitrary cross section under a constant heat flux boundary conditions. Spiga and Morini [4] investigated developing heat transfer in rectangular channels of different aspect ratios. They reported developing thermal behavior and Nusselt numbers for different combinations of heated and adiabatic walls. Kuddusi and Çetegen [5] developed a mathematical model to study thermally developed heat transfer in rectangular microchannels with constant heat flux boundary conditions. Nusselt numbers for a wide range of Knudsen numbers and aspect ratios for different combinations of heated and adiabatic walls were reported.

Another effect associated with rarefied flows is thermal creep, which can cause a velocity slip along the surface due to a tangential temperature gradient

adjacent to the wall. For cases with sufficiently high heat fluxs at the walls, axial temperature gradients can considerably influence the flow field. This is especially true for very low Reynolds number flows, where slip due to the velocity gradients is rather small.

A survey of the available literature shows a limited number of studies on thermal creep effects in microchannels. Orhan et al. [6] discussed occurrence of instabilities for thermal creep flow of rarefied gases in rectangular enclosures. Sazhin et al. [7] studied the thermal creep phenomenon through straight cylindrical capillaries in the free molecular flow regime using the DSMC method. Méolans et al. [8] developed an analytical model for thermal creep flow. They considered a planar microchannel between two reservoirs maintained at the same pressure while a constant temperature gradient was applied along the channel. Rij et al. [9] numerically studied fluid flow and heat transfer in the entrance region of a planar microchannel. Both thermally and hydrodynamically developing slip flows with prescribed constant creep velocities were investigated. They also presented an analytical solution for fully developed flow.

In the present study, incompressible gaseous slip-flows and heat transfer in the entrance region of rectangular microchannels of various aspect ratios are investigated for a prescribed constant heat flux boundary condition. Three-dimensional Navier-Stokes and energy equations along with velocity-slip and temperature-jump boundary conditions are solved numerically by a control-volume method. The effects of thermal creep and axial heat conduction are included in the analysis.

2. FORMULATION

The flow geometry is as shown in Fig. 1. The coordinate system is located in the center of the channel and the aspect ratio is denoted by $\alpha^* = 2\mathrm{h} / 2\mathrm{a}$.

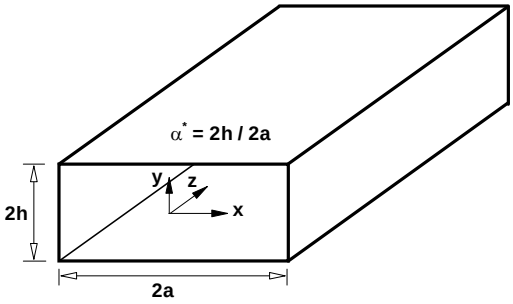

Fig. 1: Flow geometry and the coordinate system

The hydraulic diameter of the channel is set to unity and dimensions of the channel are calculated based on the channel aspect ratio and definition of hydraulic diameter as $D_h = 4(ah)/(a+h)$. Such a setting provides a more convenient base for the comparison of results since D_h is used as a length scale for non-dimensionalization. Standard integral forms of continuity, momentum and energy equations for constant-property laminar flows are used in modeling the fluid flow and thermal field as follows:

$$\int_A \vec{V} \cdot d\vec{A} = 0 \tag{1}$$

$$\frac{\partial}{\partial t}\int_\forall \rho \vec{V} d\forall + \int_\forall \rho \vec{V} \cdot \vec{\nabla} \vec{V}\, d\forall = -\int_A p d\vec{A} + \int_A \mu \vec{\nabla} \vec{V} \cdot d\vec{A} \tag{2}$$

$$\frac{\partial}{\partial t}\int_\forall \rho c_p T d\forall + \int_\forall \rho c_p \vec{V} \cdot \vec{\nabla} T d\forall = \int_A k \vec{\nabla} T \cdot d\vec{A} \tag{3}$$

where $\vec{V}$, T, ρ, p, μ, c_p and k are the velocity vector, temperature, density, pressure, dynamic viscosity, specific heat and thermal conductivity, respectively.

Inflow boundary conditions correspond to uniform flat profiles such that $w = W_m = W_i$ and $T = T_i$ where subscripts i and m refer to inlet and bulk mean conditions, respectively. For outflow, zero-gradients along the axial flow direction are applied for velocity, that is $\partial \vec{V} / \partial z = 0$. For a constant heat flux condition, the axial variation of temperature is linear far from the entrance, and therefore, a linear extrapolation is used to determine the temperature at the outlet. The pressure is set to zero at the outlet while zero pressure gradients are assigned at all other boundaries including the inlet for the mass-driven flow (Re specified) considered in the present work. The flow satisfies the velocity-slip and temperature-jump conditions at the walls, given by:

$$\mathrm{u_s} = \left(\frac{2-\sigma_\mathrm{v}}{\sigma_\mathrm{v}}\right)\lambda\left(\frac{\partial \mathrm{u}}{\partial \mathrm{n}}\right)_\mathrm{g} + \frac{3}{4}\frac{\mu}{\rho \mathrm{T_g}}\left(\frac{\partial \mathrm{T}}{\partial \mathrm{s}}\right)_\mathrm{g} \tag{4}$$

$$T_g - T_w = \left(\frac{2-\sigma_T}{\sigma_T}\right)\left(\frac{2\gamma}{\gamma+1}\right)\frac{\lambda}{\mathrm{Pr}}\left(\frac{\partial T}{\partial n}\right)_g \tag{5}$$

The other velocity components are specified similarly. Here, u_s is the slip velocity defined as $u_s = u_g - u_w$, where u_g represents the gas velocity on a wall and u_w is the wall velocity. The subscript w identifies a wall with a normal coordinate n and tangential coordinate s. The subscript g indicates the first layer of the gas adjacent to the wall where the

normal and tangential temperature gradients are evaluated. The coefficients σ_v and σ_T, known as the tangential-momentum and energy accommodation coefficients, are usually determined experimentally. They are taken as unity in the present study.

The Reynolds number, $\mathrm{Re} = \rho W_m D_h / \mu$, is based on the uniform inlet velocity and the hydraulic diameter D_h. The density is constant, and so, $W_m = W_i$ everywhere in the channel. The Knudsen number is also defined using the hydraulic diameter as $\mathrm{Kn} = \lambda / D_h$.

3. NUMERICAL METHOD

Using the control-volume method, the governing equations are integrated over corresponding finite volumes while they are transformed in a generalized non-orthogonal coordinate system. The numerical solution is based on a projection-type method that solves the momentum equations in two steps. First, an intermediate velocity field is obtained using the available pressure field. Next, velocity and pressure corrections are calculated from a Poison equation obtained from the continuity equation. The numerical scheme was originally developed by Chorin [10], and improved further by Dwyer [11] and the present authors [12]. Also, a pressure correction based on the conservation of cross sectional mass flux is introduced, which greatly enhances the convergence rate of the numerical scheme. A pressure defect for a given cross section is associated with the average velocity defect $\Delta w'$ at the same cross section according to the following equation:

$$\rho \frac{\Delta w'}{\Delta t} = -\frac{\partial p'}{\partial x} \tag{6}$$

The average velocity defect is defined as $\Delta w' = \overline{W} - W_i$ where $\overline{W}$ is the predicted cross sectional average velocity. Thus, the pressure filed is updated through the above correction and then the new velocity field is obtained using the updated pressure field.

4. Grid Independence and Validation

Numerous computations were performed to study the required cross sectional and axial grid resolutions and it was found that a mesh size of $61 \times 61 \times 121$ (x, y, z) with grid expansion ratios of about 1.06, 1.1 and 1.04 in the x, y and z directions, respectively, provide grid independent results.

The friction factors for fully developed conditions at various Knudsen numbers compare very well with the results of Morini et al. [13] as shown in Fig. 2 for three different aspect ratios.

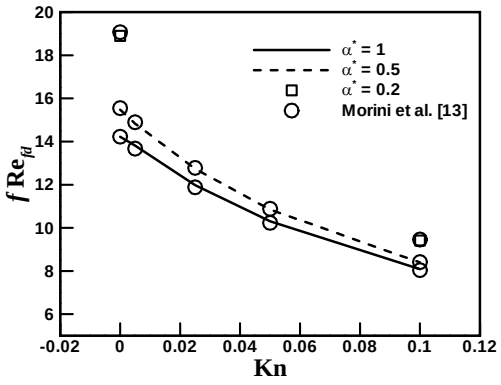

Fig. 2: Comparison of fully developed friction factor for various aspect ratios and Kn numbers.

Similarly, the fully-developed heat transfer coefficients for a constant heat flux condition have been compared with available data in a wide rang of Knudsen numbers in Fig. 3, which indicates reasonable agreement. The higher numerical predictions as compared to the published results can be attributed to axial heat conduction, which is important for the low the Reynolds number flows considered in the present study.

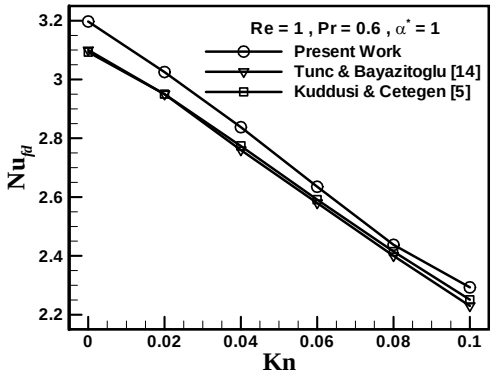

Fig. 3: Comparison of fully developed Nu number for wide range of Knudsen numbers.

For cases with thermal creep much less information is available. The fully developed friction and heat transfer coefficients in planar-microchannel flows are compared with the analytical results of Rij et al. [9] in Fig. 4, where excellent agreement is observed.

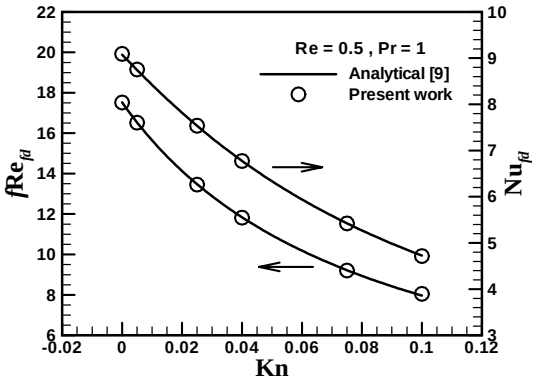

Fig. 4: Comparison of the fully developed friction and heat transfer coefficients in the presence of thermal creep for a planar microchannel.

5. RESULTS AND DISCUSSIONS

In the present study, the Prandtl number is set equal to 1 and the non-dimensional heat flux $q = q''D_h / kT_i$ is prescribes as q = 0.007. Also, $z^+ = z/(D_h\mathrm{Re})$.

5.1 The Flow Field

Thermal creep does not influence the flow field significantly at Re = 1. However, at lower Re, thermal creep can affect the slip flow pattern considerably, especially close to the channel inlet, as shown in Fig. 5 where the axial velocity contours are plotted in the symmetry plane (x = 0) for (a) Re = 1 and (b) Re = 0.1 in a square microchannel. Clearly, the developing flow pattern at Re = 0.1 is much different from that for Re = 1. Two distinct regions can be identified for the Re = 0.1 case. Close to the inlet thermal creep effects are dominant due to high axial temperature gradients and low fluid temperature at wall, and therefore, the region of high velocity is near the wall such that the uniform inlet velocity profile transforms into a parabola with the minimum velocity in the core region and maximum velocity at the wall. This is clearly seen in Fig. 6 where the evolution of the axial velocity profiles are plotted at different axial locations. For further clarity, different stages in the profile development are shown separately in Fig. 6. About 12% increase in the axial velocity component from the uniform inlet velocity occurs near the wall due to strong slip effects at the axial location of $z^+ = z/(D_h\mathrm{Re})$ = 5.162 in Fig. 6(a). However, farther down stream, where the axial temperature gradient approaches a constant value, thermal creep effects lose their strength and velocity profile converts from the inverted parabola to a flat profile (Fig. 6b, z^+ = 17.21), which latter (Fig. 6c, z^+ = 50) transforms into the conventional parabolic velocity profile with a large velocity slip of about 84% of the inlet velocity.

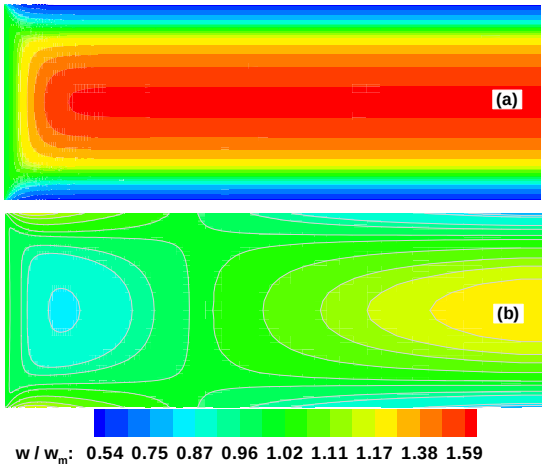

Fig. 5: Axial velocity contours in the symmetry plane of a square microchannel for Kn = 0.1, and (a) Re = 1, (b) Re = 0.1

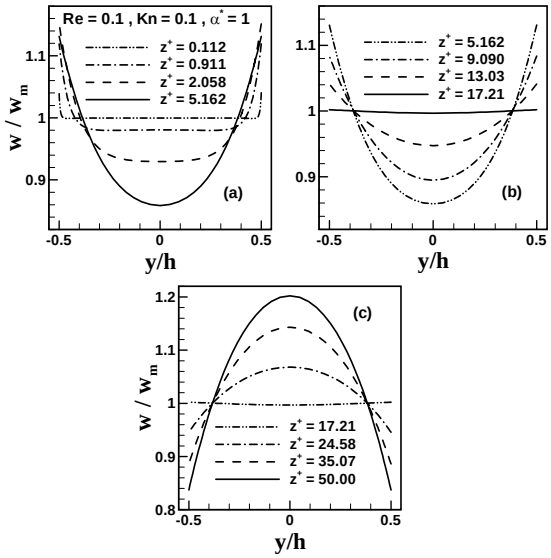

Fig. 6: Effects of thermal creep on axial velocity profiles in a square microchannel at Re = 0.1 and Kn = 0.1 at different axial locations. $z^+ = z/(D_h\mathrm{Re})$.

In Figs. 7 and 8, three dimensional streamwise velocity profiles for Re = 1 and Re = 0.1 are shown at several axial locations, respectively. These figures show the three dimensional structures of different velocity profiles in their deformation from a uniform inlet profile to their fully developed form. These velocity profiles, which are self explanatory, are cut in their symmetry plane for clarification purposes.

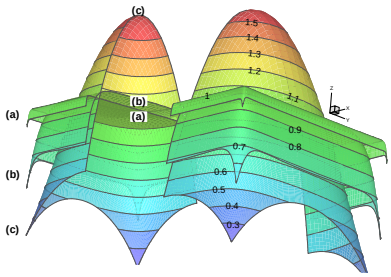

Fig. 7: The 3-D streamwise velocity profiles for Re = 1, Kn = 0.1 at axial locations: (a) z^+ = 1.052E-02, (b) z^+ = 0.104, (c) z^+ = 0.258 and z^+ = 1.007.

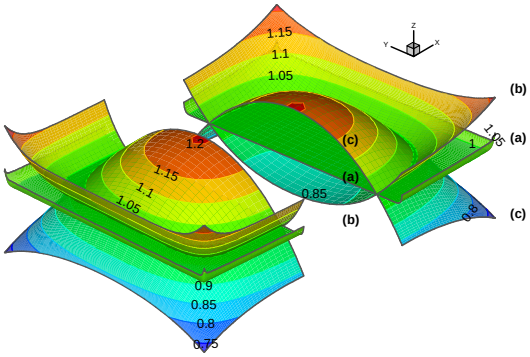

Fig. 8: The 3-D streamwise velocity profiles for Re = 0.1, Kn = 0.1 at axial locations: (a) z^+ = 1.052E-02, (b) z^+ = 0.104, (c) z^+ = 0.258 and z^+ = 1.007.

The dimensionless pressure drop along the channel is expressed in the form of an apparent friction factor defined as:

$$f_{app}\,\mathrm{Re} = \frac{1}{4z^+}\frac{\Delta\bar{p}}{\rho W_i^2/2} \tag{7}$$

where $\Delta\bar{p}$ indicates the pressure drop from the entrance. In addition to the wall shear stress, which is the only source of the pressure drop in fully developed region, the change in the momentum rate accounts for a major portion of the pressure drop in the entrance region. Figure 9 shows the variation of the apparent friction factor with Kn at Re = 1 along the channel. For comparison, cases with thermal creep are identified with a circle in this figure. Major reduction in the apparent friction coefficient in the entrance region can be attributed to two factors. Slip reduces the wall shear stresses and at the same time less pressure drop is required for transforming the velocity profile from uniform inlet profile to the fully

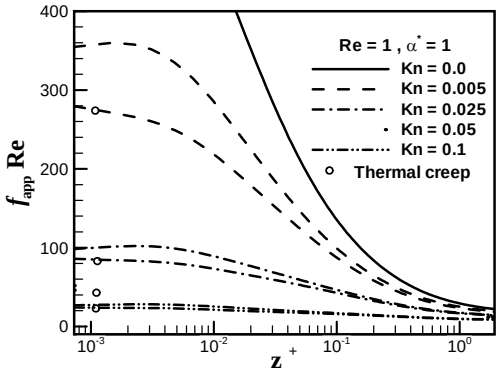

Fig. 9: Axial variation of apparent friction factors with and without thermal creep. $z^+ = z/(D_h\mathrm{Re})$.

developed profile (since fully developed velocity profiles are much flatter as compared to those with the no-slip condition). These two factors result in lower friction coefficients at higher Kn numbers. Both factors are slightly enhanced when the contribution of thermal creep is considered. The change of fully developed fRe for variation of Kn number from 0.0 to 0.1 at Re = 1 is about 44% in a square duct while this value increases to 48% for a duct with aspect ratio of 0.2. Thermal creep further reduces the fully developed friction coefficients by almost 2% for Kn = 0.1 in a square duct at Re = 1.

5.2 The Temperature Field

The temperature field in rarefied flows is a function of geometry, Re, Pr and Kn numbers. For the prescribed constant heat flux boundary condition, a dimensionless temperature can be defined as:

$$\theta = \frac{\left|T - T_{ref}\right|}{q'' D_h / k} \tag{8}$$

where T_{ref} is a reference temperature. The non-dimensional temperature profile can reveal different features depending on the choice of the reference temperature as will be discussed later. In Fig. 10, cross-sectional temperature distributions are compared for the slip and no-slip cases at Re = 1. Three different axial locations in a square microchannel are considered. For this case, the inlet temperature T_i is taken as the reference temperature and the dashed lines on the right hand side indicate the slip case with Kn = 0.1 while the solid lines refer to the no-slip case. This figure indicates almost similar temperature distributions for both the slip and no-slip flows close to the entrance, however in the fully developed region, the core is slightly warmer in the slip case as compared to the no-slip case.

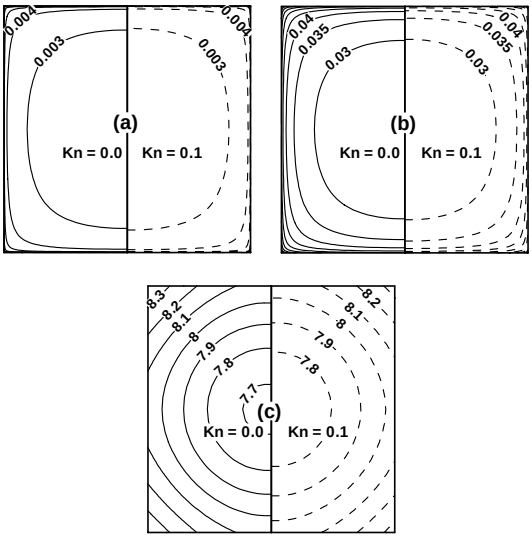

Fig. 10: Cross-sectional temperature distributions for flow in a square duct at Re = 1. Solid lines Kn = 0; dashed lines Kn = 0.1; (a) z^+ = 7.295E-4 (b) z^+ = 7.720E-3 (c) z^+ = 1.922

A better view of the entrance thermal development can be obtained through the axial variations of the temperature profiles in the symmetry plane as shown in Fig. 11. In this figure, the local wall temperature has been used as T_{ref} . Note that using T_i as the reference temperature in the definition of the non-dimensional temperature cannot reveal the temperature jump at the wall. Furthermore, non-dimensional temperature profiles based on T_i as reference temperature do not lead to a fixed profile in the fully developed region. Using local wall temperature as the reference temperature provides a base to present the wall temperature jump and leads to a fixed profile in the fully developed region. The only drawback of such a choice is that the reference temperature is not constant across the temperature field.

The effects of thermal creep on the temperature profiles are also shown in Fig. 11 where on the right half of the temperature profiles (shown by dashed lines) the thermal creep effect is included, while on the left side (shown by dotted lines) thermal creep is ignored. Despite the variation in the temperature profiles corresponding to their axial locations in the symmetry plane, the temperature jump is identical at all axial locations. This is due to the fact that local wall temperature has been used as the reference temperature along with the constant heat flux boundary condition. For such a case, temperature jump is only a function of Knudsen number.

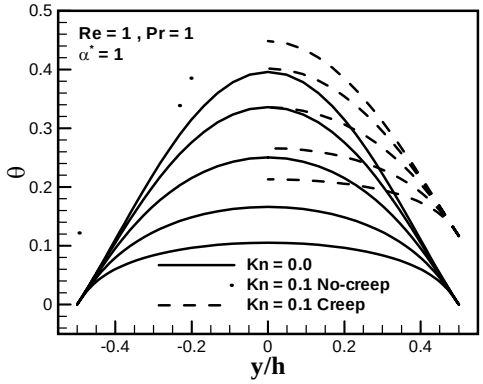

Fig. 11: Axial variation of non-dimensional temperature profiles in the symmetry plane of a square microchannel for Re = 1 in slip and no-slip flows; $z^+ = z/(D_h\mathrm{Re})$ = 5.096E-2, 0.206, 0.402 and 2.00 with increasing θ, respectively.

The maximum temperature difference Δθ between the core and the immediate vicinity of the wall is about 0.33 for Kn = 0.1, while this value increases to about 0.4 for Kn = 0. Apparently, at Re = 1, thermal creep does not affect the temperature distributions in the flow direction noticeably. However, at Re = 0.1, the temperature field is significantly influenced by thermal creep as shown in Fig. 12.

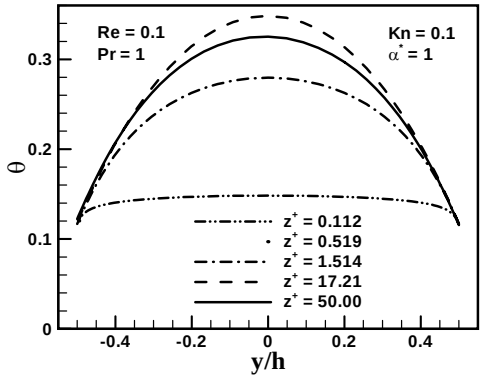

Fig. 12: Axial variation of non-dimensional temperature profiles in the symmetry plane of a square microchannel for Re = 0.1 and Kn = 0.1.

The same flow conditions and axial locations as those in Fig. 6 are used here. It is seen that the uniform inlet temperature profile undergoes a continuous transformation along the channel until it reaches its maximum value in the center corresponding to the flat velocity profile in Fig. 6(b). Farther down stream, the maximum temperature decreases gradually approaching to its fixed fully developed profile at about $z^+ = z/(D_h\mathrm{Re})$ = 50. Again, the symmetry plane is considered and local wall temperature has been

used as T_{ref} . The circumferentially-averaged local heat transfer coefficient for the peripherally uniform heat flux boundary condition is defined as:

$$Nu = \frac{h_x D_h}{k} = \frac{q'' D_h}{k\left(T_w - T_m\right)} \tag{9}$$

where T_m is the mean bulk temperature and T_w is the cross sectional averaged wall temperature defined as:

$$T_w = \frac{1}{P}\int_S T_{w,l}\, ds\,, \qquad T_m = \frac{1}{AW_i}\int_A T\vec{V}\cdot d\vec{A} \tag{10}$$

where P is the perimeter, $T_{w,l}$ is the local wall temperature, ds is a circumferential differential element and A is the cross sectional area.

Fig. 13 shows the axial variations of the heat transfer coefficients in a square microchannel for Re = 1. It is seen that the rarefaction effects dramatically reduce the heat transfer coefficient in the entrance region. There are two opposing effects regarding heat transfer. First, enhanced advection in the immediate vicinity of the wall due to velocity slip tends to increase heat transfer, and second, temperature jump at the wall which acts similar to contact resistance tends to reduce heat transfer. The net effect is a reduction in heat transfer since the temperature jump effects outweigh the enhanced advection effects. Unlike the friction coefficient, the inclusion of thermal creep, which further enhances advection, does not appear to affect the heat transfer coefficient significantly. Fully developed values of the Nusselt

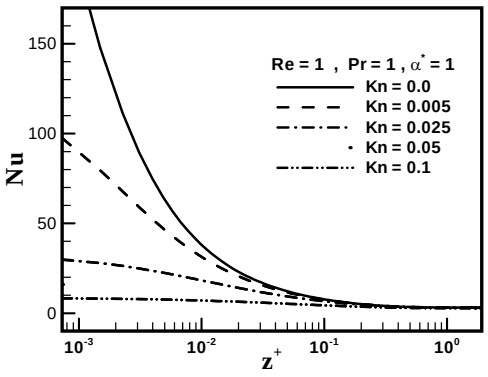

Fig. 13: Axial variation of the heat transfer coefficient for flow in a square microchannel at Re = 1 and various Kn.

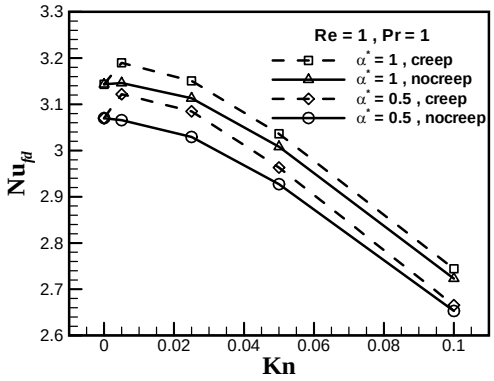

Fig. 14: Rarefaction and thermal creep effects on fully developed heat transfer coefficients

number for slip flow at Re = 1 are shown in Fig. 14 for square and rectangular microchannels with aspect ratios of 1 and 0.5, respectively. For the case of fluid heating, thermal creep is expected to increase the heat transfer rates. Yet this effect is fairly small at Re = 1 for both aspect ratios.

As discussed before, the velocity and temperature fields are very significantly influence by thermal creep at lower Reynolds numbers, and therefore, it is useful to compare the axial variation of Nu at two deferent Reynolds numbers as shown in Fig. 15, where the heat transfer coefficients are plotted for flow in a square microchannel at Re = 0.1 and 1. At lower Reynolds numbers, the increase in advection effects near the wall due to thermal creep in addition to the decrease in temperature jump (because of flatter temperature profiles) results in a considerable increase in Nu along the microchannel. In the fully developed region thermal creep at Re = 0.1 causes an increase of about 39% in the heat transfer coefficient as compared to its counterpart at Re = 1.

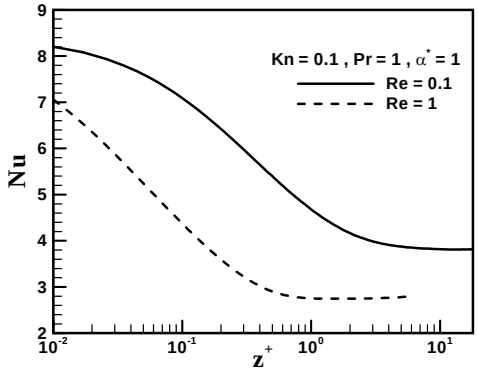

Fig. 15: Comparison of Nusselt number variation in a square microchannel at Re = 0.1 and 1.

6. CONCLUSIONS

Rarefaction and thermal creep effects on the flow and thermal development from uniform inlet profiles are numerically examined in the slip-flow regime, $Kn \leq 0.1$. Different channel aspect ratios for Reynolds numbers of 0.1 and 1 with $Pr = 1$ are considered. Developing velocity profiles and thermal patterns in the entrance region are presented in detail. The effects of thermal creep, which are directly related to the applied heat flux, are studied on the main flow parameters including the friction factor and the heat transfer coefficient. Dramatic reductions in the friction coefficient are observed in the entrance region due to rarefaction, which are enhanced by the effects of thermal creep.

Besides the axial temperature gradient at the wall, thermal creep effects are also related to the fluid heating or cooling process. For heating cases, which are considered here, it improves velocity slip at the wall, and therefore, reduces further the friction coefficient and enhances the heat transfer rates. For an identical heat flux applied to the microchannel walls, thermal creep effects become more effective at lower Reynolds number since it results in higher axial temperature gradients at the wall. Present results indicate that the flow and thermal fields are greatly influenced by thermal creep at $Re = 0.1$ under highly rarefied condition, $Kn = 0.1$. Further investigations are needed to identify the thermal creep effects in flows where the fluid is being cooled.

ACKNOWLEDGEMENT

The financial support of the Natural Sciences and Engineering Council of Canada (NSERC) is greatly appreciated.

REFERENCES

[1] D.B. Tuckerman, R.F.W. Pease, High-performance heat sinking for VLSI, IEEE Electron Dev. Lett., 2 (1981) 126-129.

[2] D.B. Tuckerman, R.F.W. Pease, Ultrahigh thermal conductance microstructures for integrated circuits, IEEE Proc. 32nd Electronics Conference, (1982) 145–149

[3] K. Hooman, A superposition approach to study slip-flow forced convection in straight microchannels of uniform but arbitrary cross-section, Heat Mass Transfer (2008), doi:10.1016/j.ijheatmasstransfer.2007.12.014.

[4] M. Spiga, G. L. Morini, The developing Nusselt numbers for slut flow in rectangular duct, Int. J. Heat and Mass Transfer, 41(1998) 2799-2807.

[5] L. Kuddusi, E. Çetegen, Prediction of temperature distribution and Nusselt number in rectangular microchannels at wall slip condition for all versions of constant heat flux, Int. J. Heat and Fluid Flow, 28 (2007) 777-786.

[6] M. Orhan, A. Ecder, A. Tezel, Stability of thermal transpiration flow in rectangular enclosures – Axisymmetric disturbances, Int. Communications in Heat and Mass Transfer, 34 (2007) 83-92.

[7] O. Sazhin, A. Kulev, S. Borisov, S. Gimelshein, Numerical analysis of gas-surface scattering effect on thermal transpiration in the free molecular regime, Vacuum, 82 (2008) 20-29.

[8] J.G. Méolans, I.A. Graur, Continuum analytical modelling of thermal creep, European Journal of Mechanics B/Fluids (2008), doi:10.1016/j.euromechflu.2008.01.005.

[9] J.V. Rij, T. Harman, T. Ameel, The effect of creep flow on two-dimensional isoflux microchannels, Int. J. Thermal Sciences, 46 (2007) 1095-1103.

[10] A.J. Chorin, Numerical solution of the Navier-Stokes equations, Math. Comput., 22 (1968) 745-762.

[11] H.A. Dwyer, Calculation of droplet dynamics in high temperature environments, Prog. Energy Combust. Sci., 15 (1989) 131-158.

[12] M. Renksizbulut, H. Niazmand, Laminar flow and heat transfer in the entrance region of trapezoidal channels with constant wall temperature, J. Heat Transfer, 128 (2006) 63-74.

[13] G.L. Morini, M. Spiga, P. Tartarini, The rarefaction effect on the friction factor of gas flow in microchannels, Superlattices and microstructures, 35 (2004) 587-599.

[14] G. Tunc, Y. Bayazitoglu, Heat transfer in rectangular microchannels, Int. J. Heat and Mass Transfer, 45 (2002) 765-773.